Journal of Superconductivity, Vol. 12, No. 2, 1999

Microwave Nonlinearities in High-T_c Superconductors: The Truth Is out There

Steven M. Anlage,[1] Wensheng Hu,[1] C. P. Vlahacos,[1] David Steinhauer,[1] B. J. Feenstra,[1] Sudeep K. Dutta,[1] Ashfaq Thanawalla,[1] and F. C. Wellstood[1]

Received 18 July 1998

This paper discusses some of the major experimental features of microwave nonlinearity in high temperature superconductors, both intrinsic and extrinsic. The case is made for solving the problem of extrinsic nonlinearity through the use of localized measurements of microwave surface impedance and electromagnetic fields. Along these lines, a brief introduction is given to our work on scanning near-field microwave microscopy.

KEY WORDS: High temperature superconductors; microwave nonlinearity.

1. INTRODUCTION

There is widespread hope that high-T_c superconducting (HTS) microwave devices will be the first to fulfill the promise of abundant everyday applications of superconductors. However, the use of HTS materials in these applications is predicated on their ability to remain linear under a variety of operating conditions. This article briefly reviews our experimental understanding of nonlinearities in HTS materials and microwave devices, and then proposes a new route to understanding and eventually controlling the microscopic causes of nonlinearity. The subject of nonlinearity in high-T_c superconductors is truly immense and beyond the scope of this paper to summarize. Instead, we will provide one perspective on this aspect of high temperature superconductivity and a simple vision for its future. The reader should be aware that many other perspectives exist on this subject and the references should be consulted whenever possible for some of these alternative ideas.

A great deal is known about the properties of HTS materials at microwave frequencies, and particularly at high power. There exist several excellent review articles [1–3] and books [4–6] on the nonlinear properties of high-T_c superconductors, and should be consulted first by newcomers to the field. We will first review the main experimental techniques used to quantify the degree of nonlinearity present in superconducting devices and materials. We then discuss the sources of nonlinearity which have been identified, concentrating on those sources of nonlinearity which are known to be extrinsic. We next discuss some empirical correlations between the material and device properties and the degree of nonlinearity. We then briefly discuss new techniques designed to characterize inhomogeneities in materials and seek out the microscopic origins of nonlinearity. Finally, we conclude with our vision for the future evolution of this field.

2. EXPERIMENTAL METHODS

Nonlinearity in superconducting devices is manifested by the fact that the device behavior is not invariant with respect to changes in the input power. Properties which change with power level include the widening of the pass band frequency range and increase of the insertion loss of a band-pass filter, or the reduction of the quality factor (Q) and shift in the resonant frequency of a high-Q superconducting resonator. Other forms of nonlinearity come from frequency conversion, and include intermodulation of two or more signals in the pass band of a filter, or

[1]Center for Superconductivity Research, Department of Physics, University of Maryland, College Park, Maryland 20742-4111.

0896-1107/99/0400-0353$16.00/0

harmonic generation in wideband devices such as delay lines. All of these manifestations of nonlinearity can be traced to the fact that the electrodynamic properties of a superconductor are fundamentally nonlinear. One direct measure of nonlinearity is how the surface impedance depends on rf power. However, more sensitive (and practical) measurements of nonlinearity exist. These include quantitative measurements of harmonic generation and intermodulation distortion. All of these characterization methods are global in the sense that the entire device is treated as a "black box." To make progress in taming nonlinearities, it is essential that we obtain a microscopic picture of the sources of nonlinearities. In Sect. 4, we discuss a new class of experimental methods which are being developed to uncover the microscopic origins of material inhomogeneity and nonlinearity.

2.1. Power-Dependent Surface Impedance

Resonant techniques are often employed to measure the surface impedance of superconductors. The surface resistance can be deduced from measurements of the Q of the resonator, while the surface reactance is found from measurements of the frequency shift of the resonator [7]. It is generally found that the surface resistance and reactance tends to increase as higher microwave powers are applied. Nonlinearity often shows up first as changes in the resonator transmission response as a function of frequency [8–11]. The surface resistance and reactance are generally observed to increase quadratically with rf field strength, H_{rf}, over a range of rf powers [12,13]. Beyond a critical rf field strength, the increase is faster than quadratic, possibly indicating heating, or a breakdown associated with the superconducting-to-normal-state transition. These measurements have the disadvantage that they are global measurements and make the assumption that the material is homogeneous. In reality, only a few areas of the film may be dominating the losses [14]. Thus, a relatively homogeneous film with a few defective areas may be judged equivalent to a homogeneously degraded film [15].

2.2. Harmonic Generation

A somewhat more sensitive measure of nonlinearity can be obtained through measurements of harmonic generation in HTS devices. In this method, a signal at frequency f_1 is applied to the device. If the device is time reversal symmetric (e.g., no trapped flux is present) then the I–V curve must obey the condition V(–I) = –V(I). If this is the case, then only odd harmonic terms can arise from nonlinearities in the I–V curve of the device [5,16]. The first (f_1) and third ($3f_1$) harmonics exiting the device are measured as a function of the input power at frequency f_1 [17–19]. It is found that with increasing field strength, harmonic generation, and intermodulation, will generally appear before one observes a change in the surface impedance [8]. A significant disadvantage of this technique is the need to create a broadband device [18], or measurement system [19], which can characterize the sample at both the fundamental and third harmonic frequencies. In addition, one obtains no detailed spatially resolved measure of where or how the harmonics are generated, except at the edges of the sample [19].

2.3. Intermodulation

The intermodulation measurement of nonlinearity overcomes the problem of device bandwidth required for harmonic generation measurements. It also has the advantage of simulating a common real-world problem associated with nonlinearity: the mixing of two or more signals to create phantom signals in the same band. In this technique, two signals at frequencies f_1 and f_2 are applied to the device, both within the passband. Typically, the difference frequency $\Delta f = f_2 - f_1$ is much less than the device bandwidth, but large enough to be outside the wings of the phase noise associated with the primary signals. The third order nonlinearity generates harmonics at frequencies $2f_1 - f_2$ and $2f_2 - f_1$ (among others), which are Δf below f_1 and Δf above f_2, respectively. Since all the signals are within the device bandwidth, no special broadband design is necessary. As the power in the primary signals is increased, the power observed in third harmonic signals generally increases three times as fast [5]. Although this characterization technique is convenient and directly relevant to such things as filter applications, it suffers once again from being a global or "black box" technique. In other words conventional intermodulation simply describes the overall nonlinearity and does not reveal local root causes of the problem.

Another problem with both harmonic generation and intermodulation measurements is that the harmonic signal often does not scale as the third power of the input signal. It is often observed that the slope of the third harmonic response vs. the input

power has a slope less than 3, or it executes an "S-shaped" pattern [18,20,21]. A proposal that the S-shaped third harmonic response is due to a redistribution of current in the device does not appear to be correct [22]. Clearly, resolution of these questions will only come from a local investigation of the sources of the third order nonlinearity.

3. THE ORIGINS OF NONLINEARITY IN HTS MATERIALS

There are four general categories of effects which cause nonlinearity in HTS materials. A good visual aid for these effects can be found in the review article mentioned above [2]. Each class is considered separately below.

3.1. Intrinsic Nonlinearity of HTS Materials

Superconductors exist because they enjoy a free energy advantage over the normal state at the same value of temperature, transport current, and magnetic field. However, this free energy advantage is finite, and can be reduced to zero by increasing the temperature, the magnetic field, or by applying a dc transport current. In the last case, a significant amount of energy can be stored in the kinetic energy of the supercurrent flow, thus reducing the free energy gain of the superconducting state. The price that is paid to transport the current is that the superconducting order parameter is suppressed. This in turn reduces the superfluid density, and hence increases the magnetic penetration depth. If still more current is carried by the superconductor, the suppression of superconducting properties is even more severe, until eventually the free energy advantage of maintaining the superconducting state is lost entirely. This process is strongly nonlinear and is intrinsic to the superconducting state.

The practical consequences of these nonlinearities usually occur only under relatively extreme conditions. Many of the effects are associated with the non-linear Meissner effect. A nonlinear Meissner effect means that a superconductor will not generate a magnetization which is strictly proportional to the applied field (as in the ideal Meissner state). Further more, in a *d*-wave superconductor, the supercurrent flowing in the directions of the nodes of the order parameter can more easily gain kinetic energy sufficient to cause depairing, and reduce the superfluid response. Because the gap increases for directions on either side of the node, the amount of depairing will depend on the strength of the applied field. One consequence of this effect is nonlinearity in the power-dependent inductance of superconducting transmission lines. For a *d*-wave superconductor, one finds that the 1 dB compression point for the kinetic inductance of a thin film (thickness less than the penetration depth) superconducting transmission line is on the order of 10^3 Oe [23]. This field scale is very high compared to H_{c1}, but may occur in situations where there is a very strong field parallel to the superconducting surface, such as in a disk resonator.

More detailed calculations by Dahm and Scalapino show that intermodulation and third harmonics are dominated by the nonlinear inductance of a *d*-wave superconductor in the intrinsic limit [24,25]. The magnitude of these nonlinearities are very small compared to the more commonly experienced extrinsic nonlinearities discussed below. One distinctive prediction of their theory is that in the presence of intrinsic *d*-wave nonlinearity, there should be an upturn in the intermodulation output at low temperatures [24,25], distinctly different from nonlinear *s*-wave superconductors, and many other forms of nonlinearity.

Another form of intrinsic nonlinearity may come from spontaneously generated trapped flux in π-junctions at high-angle grain boundaries in HTS materials [26]. This may give rise to second harmonic generation in the absence of an externally applied magnetic field [27].

3.2. Extrinsic Nonlinearities in HTS Materials

In principle, all extrinsic sources of nonlinearities in HTS materials can be controlled by careful fabrication and design. Geometrical sources of nonlinearity have been largely tamed through the use of novel disk or Corbino [28] resonator geometries. However, HTSC materials display numerous types of microscopic and mesoscopic defects, and there is still little detailed understanding of how they contribute to nonlinearity. These defects include weak links as well as other defects which cause runaway heating of the material at high powers. The central question which we must address is this: which defects are responsible for nonlinearity, which can be safely ignored, and which are actually beneficial? Once one knows which defect is responsible for the problem its effects on the surface impedance can be modelled and its presence can be reduced by altering the film growth process.

3.2.1. Geometry

In planar strip conducting structures, the spatial distribution of current flowing parallel to an edge is influenced by self magnetic fields [29]. The current density is locally increased at edges [30] and, for a given incident power, large screening currents can cause the field to exceed H_{c1}. Thus it is believed that nonlinear response starts at the edges [19]. The well-known problem of edge current buildup and subsequent breakdown of superconductivity in thin films has been attacked from many angles [30–33]. Attempts to improve the situation by tapering the edges of the film or adding normal material do not seem to help [24].

However, it is found that increasing the width of the conducting strip does help reduce the amount of nonlinearity at a given power level [18]. To further increase the power handling capabilities of HTS devices, the shape of the conductor can be changed from relatively narrow rectangular strips to patches with dimensions similar in both directions. With this geometry, the current is distributed over a larger conductor surface and the peak field strength at the edges becomes lower [21, 34]. A further refinement on this idea is the use of circular disk resonators, which are designed to excite rotationally symmetric TM_{0n0} modes. These modes offer a unique property: they carry only radial components of the current density and thus no current flows parallel to the edges [35]. Consequently, the resonators are not degraded by the "edge effect" described above. An improvement of the power handling capability by a factor of about 400, in comparison to modes with edge current, has been demonstrated [34]. Another solution to the edge current problem is to use cylindrical dielectric resonators [36,37] although they take up more volume than planar devices.

3.2.2. Weak Links

Granular superconductors exhibit enhanced nonlinearity due to "weak links" between the superconducting grains [2]. A granular HTS material is often modeled as an array of weakly Josephson-coupled superconducting grains [38–40]. A Ginzburg-Landau approach can be employed in which the array is approximated as a continuous medium characterized by effective parameters (coherence length, penetration depth, critical fields, etc.). Analogies can then be drawn between granular HTS and ordinary type-II superconductors. High-frequency losses can also be treated using a coupled-grain model in which the grains are taken to be purely inductive and the weak links are modeled using the resistively shunted junction model [41]. For weak fields, the array of superconducting grains will be screened from the applied field. When the applied field becomes large enough, flux will begin to penetrate the intergranular material from the surface [42]. Thus, the nonlinear behavior seen in granular HTS films is due to the nonlinear inductance and loss within the weak links. This implies that it is necessary to either employ single-crystal films or work with small grains which are strongly coupled to minimize the nonlinearity for high-power device applications [43–46].

An interesting extreme case of weak link microwave nonlinearity can be created by growing an HTS film on a bicrystal substrate to create a single dominant weak link. Oates and collaborators have studied the nonlinear surface impedance and intermodulation caused by such an engineered weak link in a stripline resonator [47,48]. They found that the resistively shunted junction model is successful at describing the main features of the data, as expected.

3.2.3. Thermal Effects

As materials have improved, a new source of nonlinearity has emerged: local heating and hot-spot formation. These thermal effects can arise from defects in the substrate and/or the superconducting material itself, or possibly by heating in the dielectric [21]. At high microwave current, the localized heating generated at defects may drive part of a superconductor to the normal state [49, 50]. If the small normal area blocks the path of the current, there will be a large local heating effect which may also drive surrounding material into the normal state [51]. The surface resistance will increase significantly, and the HTS film will show nonlinear properties, such as harmonic generation and intermodulation. One possible source of hot spot formation may be surface roughness, and in particular, a-axis outgrowths [52]. Efforts to deal with these outgrowths through etching of the surface have been modestly successful [53].

It appears that thermal grounding of the substrate is critical for controlling the effects of both local and global heating [14]. The differences from sample-to-sample and lab-to-lab in the high power behavior of HTS samples may be due, at least in part, to differences in thermal conductivity and the efficiency of heat extraction from the substrate [14].

3.3. Structure/Property Correlations

In the absence of a microscopic understanding of the origins of nonlinearity, one can still study empirical correlations between deposition and treatment conditions of the materials and the resulting properties of HTS devices made from those materials. As an example, Ma *et al.* found that films with a small magnetic penetration depth λ, along with good orthorhombicity in the films, yields devices which are the most linear [11]. However, this approach is very time consuming, is difficult to generalize to other methods of growing films [11], and implicitly assumes that there are no uncontrolled parameters influencing the results.

Another problem with these empirical correlations is the limited range of deposition and processing condtions over which they hold. For instance, it is found that films grown by different techniques (laser ablation, sputtering, thermal evaporation, etc.) must be separately optimized for some particular microwave property. In addition, groups which optimize different macroscopic properties for their films can end up with different microwave power handling capability. For example, one group may optimize the intermodulation products of its films because that is of interest for the end user. It is believed that this in turn optimizes the rf-field dependence of the magnetic penetration depth λ. On the other hand, another group may optimize the high power behavior of the surface resistance $R_s(H_{rf})$ for their films. These different optimization routes may well lead to different film microstructure. Clearly, microscopic characterization of the microwave properties and an understanding of superconducting current interaction with the microstructure are required.

3.4. Models of Nonlinearity

Realistic modeling of nonlinearity can only proceed after the microscopic mechanisms are identified. In the case of weak links, this process has already been advanced [41,54]. The origins of hot spots may include dust or substrate defects, although no clear candidates are known to generally occur. Other sources of nonlinearity have not been as carefully modeled. This includes, among other things, the details of the nucleation and growth of normal phase at the edge of a current-carrying strip [55]. Another important problem is the creation and motion of vortices at the edges of current-carrying superconducting strips. The formation of an rf critical state has been addressed by many authors [56,57]. Recently, the time-dependent Ginzburg–Landau equations [58] have been solved for this case [59,60]. Among other things, it is found that normal regions with multiple flux quanta can be created and move inside the film even in one half of an rf period. Further experimental work is required to see which of these models correctly describes the sources of nonlinearity in HTS materials and devices.

4. MICROSCOPIC CHARACTERIZATION

In an effort to discover the origins of nonlinearity and inhomogeneity in HTS materials, microscopic imaging techniques are being developed. These techniques fall into two classes. The first are local materials property diagnostic techniques which are designed to characterize the homogeneity and defect structure of materials. The second class are electromagnetic field (and microwave current) imaging techniques which are being applied to operating device structures to understand their high power properties. We discuss each class in turn.

4.1. Materials Property Imaging

High quality microwave devices with good power handling properties must start with high quality homogeneous superconducting materials. It is important to characterize these materials at the same frequency where they will eventually be used. In an effort to quantify and resolve the microwave properties of superconducting materials, far-field [61,62], and near-field [63–65] microwave microscopy techniques have been developed. In the most comon far-field techniques, mm-waves or light are focused on the sample and the local response is measured. Confocal resonators have been used to image losses at frequencies on the order of 100 GHz with a few mm spatial resolution [61,62]. Raman microprobe measurements have been used to characterize the oxygen loss of patterned high-T_c materials, however they do not seem to correlate with nonlinearities [22].

The near-field techniques utilize an electromagnetic radiation source in close proximity to the sample of interest. If the sample is less than one wavelength away, the ordinary concepts of far-field radiation patterns no longer apply. For instance it has been demonstrated that the spatial resolution of this sort of imaging technique can be many orders of magnitude less than the wavelength of the radiation

[66,67]. The spatial resolution is given by the larger of two experimentally controlled quantities: the probe-sample separation and the characteristic feature size which determines the field structure in the near field of the radiation source. Spatial resolutions from 10 μm [67] into the sub-μm range [68] have been demonstrated and shown to be independent of the radiation frequency [67].

Near field microwave measurements have been pursued by many groups over the years. The earliest work by Soohoo [69] and Bryant and Gunn [70] used scanned resonators with small apertures to couple to the sample of interest. The method of Ash and Nichols used an open resonator formed between a hemispherical and a planar mirror [66]. They opened a small hole in the planar mirror allowing an evanescent wave to leave the cavity (like Soohoo), and scanned a sample beneath it. As this resembles the configuration now used for near-field scanning optical microscopy, it is often reported to be the first modern near-field evanescent electromagnetic wave microscope. Near-field imaging has been accomplished using evanescent waves from the optical to the microwave range in coaxial, waveguide, microstrip, and scanning tunneling microscope geometries [71–81].

Over the past 2 years, our group has developed a novel form of near-field scanning microwave microscopy [64]. As shown in Fig. 1, our microscope consists of a resonant coaxial cable which is weakly coupled to a microwave generator on one end through a decoupling capacitor C_d, and coupled to a sample through an open-ended coaxial probe on the other end. As the sample is scanned beneath the probe, the probe-sample separation will vary (depending upon the topography of the sample), causing the capacitive coupling to the sample, C_x, to vary. This will result in a change of the resonant frequency of the coaxial cable resonator because C_x affects the electrical length of the resonator. Also, as the local sheet resistance (R_x) of the sample varies, so will the quality factor, Q, of the resonant cable because the sample (together with C_x) acts as a terminating impedance for the resonator. A low frequency feedback circuit is used to force the microwave generator to follow a single resonant frequency of the cable, and a second circuit is used to measure the Q of the resonant microscope, both in real time [82,83]. As the sample is scanned below the open-ended coaxial probe, the freqency shift and Q signals are collected simultaneously, and corresponding two-dimensional images of the sample topography and sheet resistance can be generated. The circuit runs fast enough to accurately record at scan speeds of up to 25 mm/sec.

We have demonstrated that our scanning near-field microwave microscope can be used to obtain quantitative topographic images with 55 nm vertical sensitivity [84], and quantitative surface sheet resistance images of metallic thin films [83]. Figure 2 shows

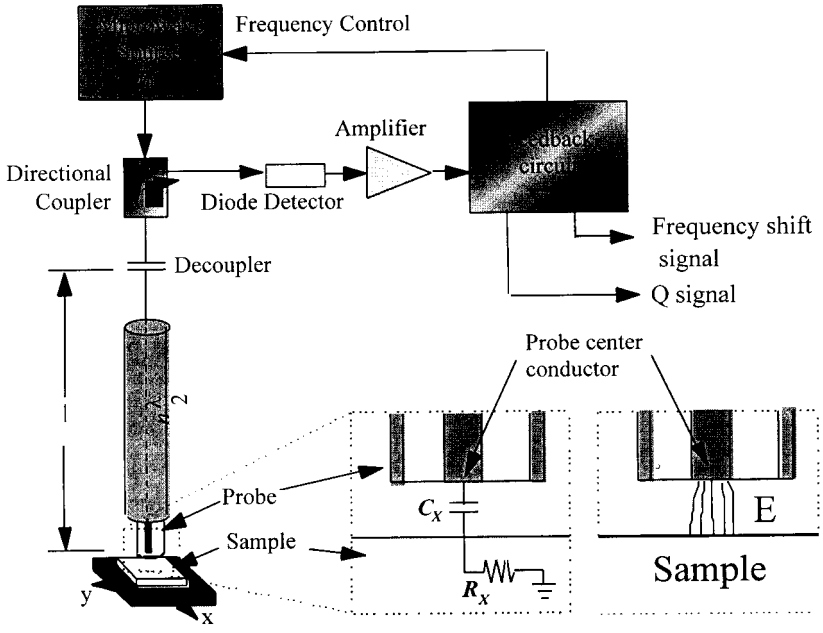

Fig. 1. Schematic of our scanning near-field microwave microscope. The microwave source is frequency locked to one of the resonant modes of the coaxial transmission line resonator. The sample perturbs one end of the resonator, and the resulting change in resonant frequency and quality factor are recorded as a function of the position of the probe over the sample.

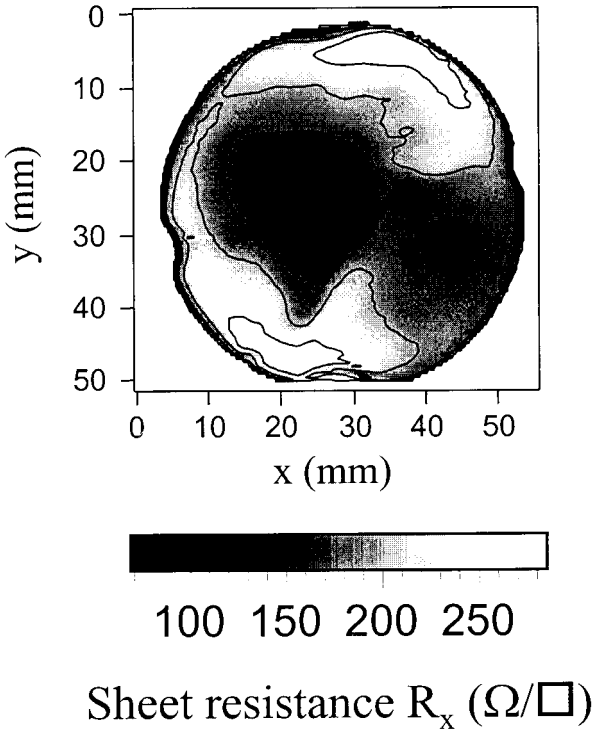

Fig. 2. Calibrated sheet resistance image of a $YBa_2Cu_3O_7$ thin film deposited on a 2-inch diameter sapphire wafer. The image was acquired at 7.5 GHz with a 480 μm diameter probe at a height of 50 μm at room temperature.

a microwave frequency sheet resistance image of a $YBa_2Cu_3O_7$ thin film deposited on a 2-in diameter sapphire wafer [85]. The film shows a sheet resistance which varies by a factor of 3 over its surface. The image has a spatial resolution of approximately 500 μm, and was obtained at room temperature in only 10 min. Such a simple technique could provide a rapid screening method for wafer-scale homogeneity.

A microwave microscope can probe the material on many different length scales, allowing one to address a host of issues from large scale homogeneity to the effect of sample microstructure on the microwave properties. Higher spatial resolution images have been achieved using coaxial probes with inner conductor diameters of 200 μm, 100 μm, and 10 μm. We have also demonstrated the ability to image with an STM-tip center conductor coaxial cable probe. With this probe we have demonstrated a spatial resolution on the order of 1 μm or better while in contact with the surface. Our microscope also has a broad frequency coverage (100 MHz to 50 GHz) allowing us to explore the frequency dependence of microwave properties and, in principle, to perform conductivity depth profiling experiments.

4.2. Electromagnetic Field and Current Imaging

Near-field microwave microscopes can also be used to image electromagnetic fields. Several groups have demonstrated electric field [86–88] and magnetic field [89] imaging above operating microwave devices using near-field techniques. In addition several groups have developed (far field) scanning laser [35,90] and electron [91] microscopes which can image microwave currents on the few μm length scale. Images from such systems can form the basis for investigating the interaction of the microwave currents with the microstructure of the materials making up the device.

Our microscope can also be used to image electric and magnetic fields in the vicinity of operating microwave devices. Figure 3 illustrates how we use the open-ended coaxial probe to pick-up electric fields above an operating device. The microscope detects the normal component of electric field, i.e., the electric field integrated over the exposed area of the center conductor of the probe. Thus the spatial resolution is again limited by the same geometrical parameters which are present in materials diagnostic mode. The picked up signals are then stored in the resonant system, rectified by a diode, and recorded on a computer [67,88,92].

We have imaged a variety of devices using this system. For example, Fig. 4a shows a short microstrip transmission line lithographically defined on a two-sided copper printed circuit board which terminates at an open circuit on the right-hand side. The

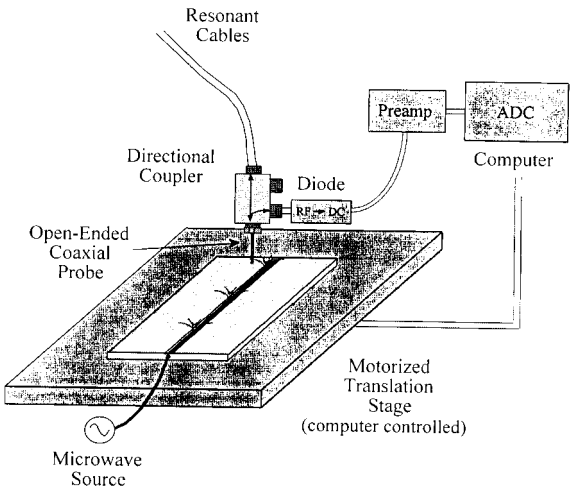

Fig. 3. Schematic illustration of scanning near-field microwave microscope operated as an electric field microscope over an active device. The open-ended coaxial probe is sensitive of the electric field normal to the surface of the inner conductor.

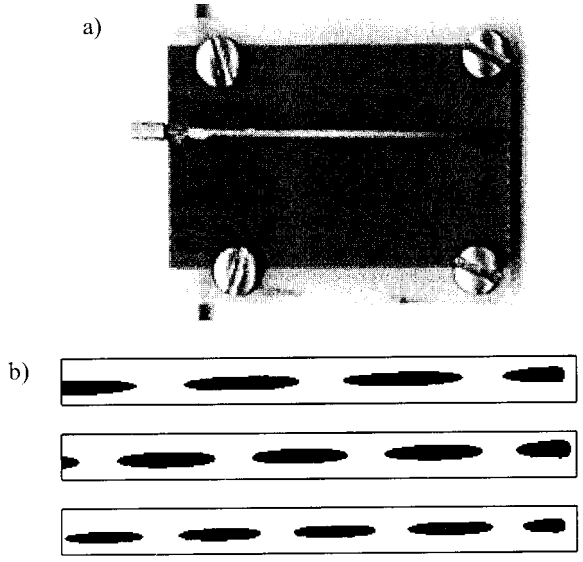

Fig. 4. (a) Optical photograph of a copper microstrip circuit showing coax-to-microstrip transition on left, and open circuit termination on right. The printed circuit board is 39 mm long and 33 mm wide, and the line is approximately 1 mm wide. (b) The lower part of the figure shows active images of the copper microstrip with standing waves present. Operating frequencies are (from top to bottom) 8.03 GHz, 9.66 GHz, and 11.29 GHz. The horizontal scale is 32.5 mm and the vertical scale on each panel is 3 mm.

strip is approximately 1-mm wide, and the dielectric is 0.5-mm thick. Figure 4b shows three active mode images of the microstrip taken at 8.03, 9.66, and 11.29 GHz with a signal applied through the coaxial cable on the left. The image is taken over the right two-thirds of the microstrip shown in Fig. 4a. In each case there is a maximum signal on the right hand side at the position of the open termination demonstrating that, as expected, the microscope is sensitive to the absolute magnitude of the electric field rather than current. A clear-standing wave pattern is seen in each image, with a wavelength which decreases linearly with increasing frequency. Analysis of the three images gives effective dielectric constants for the printed circuit board microstrip in the range of 3.32–3.46. We have also developed a technique to determine the approximate value of the perturbed electric field measured by this microscope [88,92].

The microscope is sensitive to the component of electric field normal to the microstrip circuit plane. The image (Fig. 4b) demonstrates clearly that there are standing waves on the transmission line, and will be of great assistance in the design of new planar microwave devices (both normal and superconducting). A cryogenic version of this microscope has been used to image the electric fields above a superconducting $Tl_2Ba_2CaCu_2O_8$ microstrip resonator operating at 8 GHz and 77 K [88].

There are a number of technical issues which need to be addressed before we can exploit these microscopes to their fullest potential. The first concerns the perturbation on the device caused by the presence of the measurement probe. This perturbation may be so great as to change the current distributions and obscure the actual behavior. A second issue concerns the challenge of simultaneously obtaining the required spatial resolution, topographic information, low temperature operation, and quantitative imaging capability on an operating microwave device. Both of these challenges call for continued research by the microwave microscopy community.

5. CONCLUSIONS

The elimination or control of nonlinearities in HTS materials will require a microscopic understanding of the defects and geometrical features which produce extrinsic forms of nonlinearity. We believe that the best route to this goal is through a quantitative microscopic imaging of materials properties, electromagnetic fields, and currents, at microwave frequencies and cryogenic temperatures. Near-field scanning microwave microscopy is uniquely suited to achieve this goal. We look forward to continued progress in achieving higher spatial resolution with quantitative cryogenic imaging capabilities.

The research opportunities for microwave microscopes are virtually unlimited. We hope that it will soon be possible to combine electromagnetic field imaging with simultaneously acquired topographic information [87] in the superconducting state. This will allow us to see for the first time the interactions between microwave currents and the rich and widely varying microstructure of the HTS materials. This in turn may allow us to understand which defects are specifically responsible for particular nonlinearity features. It may then be possible to eliminate or mitigate the effects of those particular defects to improve the power handling capabilities of HTS devices.

The use of ideal model systems to understand and model the microscopic origins of nonlinearity is particularly important. There has been tremendous progress made in the understanding of Josephson vortex motion at high frequencies through the use of single grain boundary weak link stripline resonators. Similar experiments can be done with other idealized

sources, such as thermal defects, tailored edge geometries, and multiple weak link structures. These experiments need to be accompanied by detailed models which explain the basic physics of the nonlinearity process. Armed with this information, it is then possible, in principle, to create films which do not suffer from those forms of extrinsic nonlinearity and to achieve the goal of HTS microwave applications free of extrinsic limitations.

ACKNOWLEDGMENTS

We would like to acknowledge many important conversations on this subject with Jurgen Halbritter and R. B. Hammond. This work was sponsored by the National Science Foundation through grant #ECS-96-32811, and the NSF/Maryland MRSEC grant #DMR-96-32521. Additional support has come from the Maryland Center for Superconductivity Research.

REFERENCES

1. N. Newman and W. G. Lyons, *J. Supercond.* **6**, 119 (1993).
2. T. B. Samoilova, *Supercond. Sci. Technol.* **8**, 259 (1995).
3. M. A. Hein, in *Studies of High-Temperature Superconductors*, Vol. 18, A. Narlikar, ed. (Nova Sciences, New York, 1996), p. 141.
4. A. M. Portis, *Electrodynamics of High-Temperature Superconductors* (World Scientific, Singapore, 1993).
5. Z.-Y. Shen, *High Temperature Superconducting Microwave Circuits* (Artech House, Boston, 1994).
6. M. J. Lancaster, *Passive Microwave Device Applications of High Temperature Superconductors* (Cambridge University Press, 1997).
7. O. Klein, S. Donovan, M. Dressel, and G. Gruner, *Int. J. Infrared Millimeter Waves* **14**, 2423 (1993); S. Donovan, O. Klein, M. Dressel, K. Holczer, and G. Gruner, *Int. J. Infrared Millimeter Waves* **14**, 2459 (1993); M. Dressel, O. Klein, S. Donovan, and G. Gruner, *Int. J. Infrared Millimeter Waves* **14**, 2489 (1993).
8. C. C. Chin, D. E. Oates, G. Dresselhaus, and M. S. Dresselhaus, *Phys. Rev. B* **45**, 4788 (1992).
9. B. A. Willemsen, J. S. Derov, J. H. Silva, and S. Sridhar, *IEEE Trans. Appl. Supercond.* **5**, 1753 (1995); T. Jacobs, B. A. Willemsen, and S. Sridhar, *Rev. Sci. Instr.* **67**, 3757 (1996).
10. H. J. Snortland, PhD thesis, Stanford University (1997).
11. Z. Ma *et al.*, *IEEE Trans. Appl. Supercond.* **7**, 1911 (1997).
12. D. E. Oates, A. C. Anderson, and P. M. Mankiewich, *J. Supercond.* **3**, 251 (1990).
13. D. E. Oates *et al.*, *J. Supercond.* **5**, 363 (1992).
14. M. A. Hein *et al.*, *J. Supercond.* **10**, 109 (1997).
15. A. N. Reznik, *IEEE Trans. Appl. Supercond.* **7**, 1474 (1997).
16. L. Ji, R. H. Sohn, G. C. Spalding, C. J. Lobb, and M. Tinkham, *Phys. Rev. B* **40**, 10936 (1989).
17. M. Golosovsky, D. Davidov, E. Farber, T. Tsach, and M. Schieber, *Phys. Rev. B* **43**, 10390 (1991).
18. C. Wilker *et al.*, *IEEE Trans. Appl. Supercond.* **5**, 1665 (1995).
19. G. Hampel *et al.*, *Appl. Phys. Lett.* **71**, 3904 (1997).
20. W. Diete *et al.*, *IEEE Trans. Appl. Supercond.* **7**, 1236 (1997).
21. Z.-Y. Shen *et al.*, *IEEE Trans. Appl. Supercond.* **7**, 2446 (1997).
22. K. E. Myers *et al.*, *IEEE Trans. Appl. Supercond.* **7**, 2126 (1997).
23. J. Mao, S. M. Anlage, J. L. Peng, and R. L. Greene, *IEEE Trans. Appl. Supercond.* **5**, 1997 (1995).
24. T. Dahm and D. J. Scalapino, *J. Appl. Phys.* **81**, 2002 (1997).
25. T. Dahm and D. J. Scalapino, *J. Appl. Phys.* **82**, 464 (1997).
26. J. Mannhart *et al.*, *Phys. Rev. Lett.* **77**, 2782 (1996).
27. Richard Humphreys, private communication (1998).
28. J. C. Booth, D. H. Wu, and Steven M. Anlage, *Rev. Sci. Instr.* **65**, 2082 (1994).
29. D. M. Sheen *et al.*, *IEEE Trans. Appl. Supercond.* **1**, 108 (1991).
30. B. A. Willemsen, T. Dahm, and D. J. Scalapino, *Appl. Phys. Lett.* **71**, 3898 (1997).
31. B. B. Jin *et al.*, *Supercond. Sci. Technol.* **8**, 564 (1995).
32. C. W. Lam, D. M. Sheen, S. M. Ali, and D. E. Oates, *IEEE Trans. Appl. Supercond.* **2**, 58 (1992).
33. L. H. Lee, S. M. Ali, and W. G. Lyons, *IEEE Trans. Appl. Supercond.* **2**, 49 (1992).
34. H. Chaloupka, M. Jeck, B. Gurzinski, and S. Kolesov, *Electr. Lett.* **32**, 1735 (1996).
35. T. Kaiser, M. A. Hein, G. Muller, and M. Perpeet, *Appl. Phys. Lett.* **73**, 3447 (1998).
36. Z.-N. Shen *et al.*, *IEEE Trans. Microwave Theory Technol.* **40**, 2424 (1992).
37. W. Diete *et al.*, 1995 EUCAS Conference Proceedings.
38. T. L. Hylton *et al.*, *Appl. Phys. Lett.* **53**, 1343 (1988).
39. C. Attanasio, L. Maritato, and R. Vaglio, *Phys. Rev. B* **43**, 6128 (1991).
40. J. McDonald and John R. Clem, *Phys. Rev. B* **56**, 14723 (1997).
41. J. S. Herd, D. E. Oates, and J. Halbritter, *IEEE Trans. Appl. Supercond.* **7**, 1299 (1997).
42. J. Wosik *et al. Phys,. Rev. B* **51**, 16289 (1995).
43. J. Halbritter, *J. Appl. Phys.* **68**, 6315 (1990).
44. C. C. Chin, D. E. Oates, G. Dresselhaus, and M. S. Dresselhaus, *Phys. Rev. B* **45**, 4788 (1992).
45. J. Halbritter, *J. Supercond.* **8**, 691 (1995).
46. T. Yoshitake, H. Tsuge, and T. Inui, *IEEE Trans. Appl. Supercond.* **5**, 2571 (1995).
47. D. E. Oates *et al.*, *Appl. Phys. Lett.* **68**, 705 (1996).
48. T. C. L. G. Sollner, J. P. Sage, and D. E. Oates, *Appl. Phys. Lett.* **68**, 1003 (1996).
49. M. A. Golosovsky, H. J. Snortland, and M. R. Beasley, *Phys. Rev. B* **51**, 6462 (1995).
50. J. Wosik *et al.*, *J. Supercond.* **10**, 97 (1997).
51. W. J. Skocpol, M. R. Beasley, and M. Tinkham, *J. Appl. Phys.* **45**, 4054 (1974).
52. Y. J. Tian *et al.*, *Appl. Phys. Lett.* **65**, 2356 (1994).
53. A. Roshko *et al.*, *IEEE Trans. Appl. Supercond.* **5**, 1733 (1995).
54. A. M. Portis, *Appl. Phys. Lett.* **58**, 307 (1991).
55. A. B. Kozyrev *et al.*, *Supercond. Sci. Technol.* **7**, 777 (1994).
56. S. Sridhar, *Appl. Phys. Lett.* **65**, 1054 (1994).
57. Shu-Ang Zhou, *SPIE Proc.* **2559**, 47 (1995).
58. M. Tinkham, *Introduction to Superconductivity* (McGraw-Hill, New York, 1974), p. 250.
59. I. Aronson, R. Gitterman, and B. Ya. Shapiro, *Phys. Rev. B* **51**, 3092 (1995).
60. I. Aronson, B. Ya. Shapiro, and V. Vinokur, *Phys. Rev. Lett.* **76**, 142 (1996).
61. J. S. Martens *et al.*, *Appl. Phys. Lett.* **58**, 2543 (1991).
62. W. L. Holstein, L. A. Parisi, Z. Y. Shen, C. Wilker, M. S. Brenner, and J. S. Martens, *J. Supercond.* **6**, 191 (1993).
63. M. Golosovsky and D. Davidov, *Appl. Phys. Lett.* **68**, 1579 (1996).
64. C. P. Vlahacos, R. C. Black, S. M. Anlage, and F. C. Wellstood, *Appl. Phys. Lett.* **69**, 3272 (1996).
65. Y. Lu *et al.*, *Science* **276**, 2004 (1997).
66. E. A. Ash and G. Nichols, *Nature* **237**, 510 (1972).

67. S. M. Anlage *et al.*, *IEEE Trans. Appl. Supercond.* **7**, 3686 (1997).
68. C. Gao, T. Wei, F. Duewer, Y. Li, and X.-D. Xiang, *Appl. Phys. Lett.* **71**, 1872 (1997).
69. R. F. Soohoo, *J. Appl. Phys.* **33**, 1276 (1962).
70. C. A. Bryant and J. B. Gunn, *Rev. Sci. Instr.* **36**, 1614 (1965).
71. U. Durig, D. W. Pohl, and F. Rohmer, *J. Appl. Phys.* **59**, 3318 (1986).
72. R. J. Gutman, J. M. Borrego, P. Chakrabarti, and Ming-Shan Wang, *IEEE MTT-S Dig.* 281 (1987).
73. M. Tabib-Azar, N. S. Shoemaker, and S. Harris, *Meas. Sci. Technol.* **4**, 583 (1993).
74. T. Wei, X. D. Xiang, W. G. Wallace-Freedman, and P. G. Schultz, *Appl. Phys. Lett.* **68**, 3506 (1996).
75. G. Nunes and M. R. Freeman, *Science* **262**, 1029 (1993).
76. R. J. Hamers and D. G. Cahill, *Appl. Phys. Lett.* **57**, 2031 (1990).
77. W. Seifert, E. Gerner, M. Stachel, and K. Dransfeld, *Ultramicroscopy* **42–44**, 379 (1992).
78. I. Takeuchi *et al.*, *Appl. Phys. Lett.* **71**, 2026 (1997).
79. S. J. Stranick, L. A. Blumm, M. M. Kamma, and P. S. Weiss, in *Photons and Local Probes*, O. Marti and R. Miller, eds. (Kluwer, Netherlands, 1995), p. 221.
80. F. Keilmann, D. W. van der Weide, T. Eickelkamp, R. Merz, and D. Stakle, *Opt. Commun.* **129**, 15 (1996).
81. M. Fee, S. Chu, and T. W. Hansch, *Opt. Commun.* **69**, 219 (1989).
82. D. E. Steinhauer, C. P. Vlahacos, Sudeep Dutta, F. C. Wellstood, and S. M. Anlage, *Appl. Phys. Lett.* **71**, 1736 (1997).
83. D. E. Steinhauer, C. P. Vlahacos, S. K. Dutta, B. J. Feenstra, F. C. Wellstood, and S. M. Anlage, *Appl. Phys. Lett.* **72**, 861 (1998).
84. C. P. Vlahacos, D. E. Steinhauer, S. K. Dutta, B. J. Feenstra, Steven M. Anlage, and F. C. Wellstood, *Appl. Phys. Lett.* **72**, 1778 (1998).
85. Color images of our microwave microscopy work are available at http://www.csr.umd.edu/research/hifreq/micr_microscopy.html
86. T. P. Budka, S. D. Waclawik, and G. M. Rebeiz, *IEEE Trans. MTT* **44**, 2174 (1996).
87. D. W. van der Weide and P. Neuzil, *J. Vac. Sci. Technol. B* **14**, 4144 (1996).
88. A. Thanawalla *et al.*, *Appl. Phys. Lett.* **73**, 2491 (1998).
89. V. Agrawal, P. Neuzil, and D. van der Weide, *Appl. Phys. Lett.* **71**, 2343 (1997).
90. H. S. Newman and J. C. Culbertson, *Microwave Opt. Technol. Lett.* **6**, 725 (1993).
91. R. Gerber *et al.*, *Appl. Phys. Lett.* **66**, 1554 (1995).
92. S. K. Dutta *et al.*, *Appl. Phys. Lett.* **74**, 156 (1999).